Dynamic Mechanical, Rheological, and Thermal Properties of Intercalated Polystyrene/Organomontmorillonite Nanocomposites: Effect of Clay Modification on the Mechanical and Morphological Behaviors

Sanjay K. Nayak, Smita Mohanty

Laboratory for Advanced Research in Polymeric Materials, Central Institute of Plastics Engineering and Technology, Bhubaneswar 751 024, India

Received 13 July 2006; accepted 6 July 2008
DOI 10.1002/app.29437
Published online 23 January 2009 in Wiley InterScience (www.interscience.wiley.com).

ABSTRACT: Polystyrene (PS)/organomontmorillonite nanocomposites were prepared by melt processing with a twin-screw extruder. Sodium montmorillonite was organically modified with stearyl trimethyl ammonium chloride to evaluate the effect of clay modification on the performance of the nanocomposites. A comparative account of nanocomposites prepared with the commercial clay Cloisite 20A (C20A) is presented. X-ray diffraction studies indicated that the clay layers were completely dispersed, and a delaminated structure was formed in the case of C20A/PS and organomontmorillonite/PS nanocomposites. The dispersion characteristics of the clays within the matrix polymer were further investigated through transmission electron microscopy analysis. Mechanical tests revealed increases in the tensile, flexural, and impact strengths of 83, 55, and 74%, respectively, for C20A/PS nanocomposites at a 5% clay loading. The viscoelastic response of the nanocomposites, studied with dynamic mechanical analysis, also showed a substantial increase in the storage modulus of the nanocomposites with the incorporation of organically modified nanoclays. Furthermore, the melt-state rheology of the organically modified nanocomposites displayed three distinct regions—glassy, plateau, and terminal—from the high-frequency region to the low-frequency region, with a considerable increase in the storage modulus in the glassy and terminal regions. Differential scanning calorimetry and thermogravimetric analysis were also used to evaluate the effect of the addition of nanoclays on the glass-transition temperature and thermal stability of the PS matrix. J Appl Polym Sci 112: 778–787, 2009

Key words: glass transition; mechanical properties; organoclay; polystyrene; TEM

INTRODUCTION

Polymer/organically modified layered silicate nanocomposites are a new class of filled polymers with ultrafine phase dimensions. These materials have widened the range of applications in areas such as the automotive, aerospace, transportation, and construction industries and electronic products.[1,2] Besides dramatically improving the mechanical, thermal, and gas-barrier properties and flame retardancy, polymer/clay nanocomposites exhibit unusual chemical and physical phenomena such as high anisotropy, electrical conductivity, and photoactivity.[1–3]

These nanocomposites are synthesized through the blending of an organically modified layered silicate into a polymer melt. Thus, understanding the relationship between the molecular structure and the thermal stability of the organic modification of the layered silicate is critical.[4–6] Two particular characteristics of layered silicates are exploited in the preparation of nanocomposites. The first is the fact that layered clays can be easily dispersed into individual layers of 1-nm thickness, and the second is their ability to alter the surface chemistry through cation-exchange reactions.

Extensive investigations have focused primarily on the modification of clays,[7–9] intercalation of a suitable monomer followed by polymerization,[10] polymer intercalation from a solution,[11] and direct melt intercalation[12–14] to fabricate nanocomposites with desired attributes. Several useful polymer/clay nanocomposites involving various thermoplastic matrices such as nylon-6/66,[15–17] polystyrene (PS),[18,19] polyolefins,[20] and poly(methyl methacrylate)[21,22] have been successfully synthesized. These nanocomposites have been found to exhibit drastic improvements in mechanical and thermal properties that are generally attributed to the uniform dispersion of clay smectite layers within the polymer

Correspondence to: S. K. Nayak (drsknayak@gmail.com).
Contract grant sponsor: Department of Science and Technology (Young Scientist Award of the Science and Engineering Research Council to S.M.).

matrix. The impregnation of clay in a styrene monomer, followed by polymerization, is a commonly used method reported by various workers. Kato et al.[23] studied the intercalation of PS in stearyl trimethyl ammonium cation-exchanged montmorillonite (MMT) by *in situ* polymerization. PS intercalated nanocomposites prepared with a vinyl benzyl trimethyl ammonium chloride compound for an organophilic ion-exchange reaction with MMT in the presence of acetonitrile were synthesized by Akelah and Moet.[24] A maximum d_{001}-spacing of 2.54 mm has been reported. Giannelis et al.[18] developed a new method for producing PS/clay nanocomposites by a melt intercalation technique. Xaoan and Syed[25] used vinyl benzyl dimethyl dodecyl ammonium chloride as a swelling agent for clay intercalation and added azobisisobutyronitrile to initiate polymerization from a swelling agent with a styrene monomer. Similarly, nanocomposites of styrene and MMA by bulk, solution, suspension, and emulsion polymerization were studied by Zhu et al.[26] Tanque et al.[27] investigated the degree of dispersion and oxidative degradation of different grades of PS with organoclay. Decreases in the storage and loss moduli with an increase in the strain have been reported. Similar studies on PS/clay nanocomposites have also been described.

This study reports the effect of the organic modification of nanoclays on the performance of PS nanocomposites. PS/organomontmorillonite (OMMT) nanocomposites were prepared by a melt processing technique in a twin-screw extruder. Stearyl trimethyl ammonium chloride (STAC) was used as a surfactant for the organic modification of sodium montmorillonite (Na-MMT). A systematic study on the effect of the clay loading on the mechanical and thermal properties of the nanocomposites was made. The extent of intercalation and dispersion of the clays within the PS matrix was evaluated with X-ray diffraction (XRD) and transmission electron microscopy (TEM). The nanocomposites were also subjected to dynamic mechanical analysis (DMA) to examine the viscoelastic behavior of the materials under periodic stress. The melt-state rheological properties of the matrix polymer as well as the nanocomposites were also studied in the linear viscoelastic range. The melting temperature and thermal stability of the nanocomposites were also studied with differential scanning calorimetry (DSC) and thermogravimetric analysis (TGA).

EXPERIMENTAL

Materials

PS (SC 203LV) with a density of 1.05 g/cc and a melt flow index of 8 g/10 min, obtained from M/s Supreme Petrochem, Ltd. (Mumbai, India), was used as the base polymer matrix.

Na-MMT with a cation-exchange capacity of 92.6 milliequiv/100 g of clay and a *d*-spacing of 1.1.7 nm, obtained from Southern Clay Co. (Gonzales, TX), was used as a reinforcing agent to prepare untreated nanocomposites.

MMT, pretreated with di(hydrogenated tallow alkyl) dimethyl ammonium chloride and supplied by Southern Clay under the trade name Cloisite 20A (C20A), was used as a treated clay to prepare treated nanocomposites.

STAC was obtained from M/s Zhangjiagang Luyuan Organic Chemical Co., Ltd. (Shanghai, China) as a gift sample and was used as a surfactant to prepare OMMT in the laboratory. All other reagents were analytical-reagent-grade and were used without further purification.

Modification of Na-MMT

The modification of Na-MMT was carried out according to the procedure reported by Hwu et al.[28] Na-MMT (10 g) was added to 600 mL of a STAC solution and 0.5 mL of concentrated orthophosphoric acid. The resultant mixture was stirred at 80°C for 24 h. Subsequently, a white precipitate was isolated by filtration, washed thoroughly with the reaction solvent (deionized water), and finally dried *in vacuo* for 8 h to obtain treated clays designated as OMMT.

Compounding

The melt blending of PS and nanoclays (Na-MMT, C20A, and OMMT) of different weight percentages (0.5, 1, 3, and 5) was carried out in an intermeshing, counter-rotating twin-screw extruder (ctw-100, Haake, GmbH, Karlsruhe, Germany) with a barrel length of 300 mm and an angle of entry of 90°. Before extrusion, the matrix polymer and the nanoclays were dehumidified in a vacuum oven at 80°C for a period of 4 h. Virgin PS along with nanoclays of different weight percentages was fed at the rate of 5 kg/h through the hopper. The process was carried out at the screw speed of 50–60 rpm and with a temperature difference of 190, 200, and 210°C between the feed zone and die zone. Finally, the extrudate was cooled in water at room temperature, granulated in a pelletizer (Fisons, Germany), and dried.

Specimen preparation

Subsequently, these granules were used for the preparation of standard rectangular bars and dumbbell-shaped specimens according to ASTM D with an injection-molding machine (ES300/80HL, Engel, Schwertberg, Austria) that had a clamping force of

800 kN and a maximum swept volume of 254 cm^3 and was fitted with a dehumidifier (Bry-Air, United States) in the temperature range of 60–80°C. The specimens were molded in the temperature range of 195–210°C.

Characterization

Morphology

XRD. X-ray diffractograms of Na-MMT, C20A, OMMT, and the nanocomposites were recorded with a Philips (Osaka, Japan) X'Pert MPD X-ray crystallographic unit equipped with a nickel-filtered Cu Kα radiation source operated at 40 kV and 40 mA. The basal spacing or d_{001} reflection of the samples was calculated with Bragg's equation through the monitoring of the diffraction angle (2θ) from 2 to 10°.

TEM. The morphology of the nanocomposites was observed with a JEOL (Tokyo, Japan) JSM 2000FX electron microscope with a 200-kV accelerating voltage. Ultrathin specimens of 100-nm thickness were cut from the middle section of a compression-molded bar with a Reichart Ultracut microtome (Leica, Milton Keynes, UK). The specimens were collected on a trough filled with water and placed on 200-mesh grids.

Mechanical properties

Test specimens for analyzing mechanical properties were initially conditioned at 23 ± 1°C and 55 ± 2% relative humidity for 24 h before testing. These conditioned specimens were subjected to mechanical testing, and an average of five measurements was reported. The corresponding standard deviation along with the measurement uncertainty value for the experimental data showing the maximum deviation is also included.

Tensile testing. Specimens of virgin PS and the nanocomposites with dimensions of 165 × 13 × 3 mm^3 were subjected to tensile testing according to ASTM D 638 with a universal testing machine (LR 100K, Lloyds Instruments, Ltd., Leicester, UK) at a crosshead speed of 50 mm/min and with a gauge length of 50 mm.

Flexural testing. The nanocomposites along with virgin PS specimens with dimensions of 80 × 12.7 × 3 mm^3 were taken for flexural testing under three-point bending with the same universal testing machine in accordance with ASTM D 790 at a crosshead speed of 1.3 mm/min and with a span length of 50 mm.

Impact testing. The Izod impact strength was also determined from specimens with dimensions of 63.5 × 12.7 × 3 mm^3. The tests were carried out with a model 6545 impact meter (Ceast, Pianezza, Italy) according to ASTM D 256 with a notch angle of 45° and a V-notch depth of 2.54 mm.

DMA

Specimens of virgin PS and the nanocomposites with dimensions of 35 × 12 × 3 mm^3 were subjected to dynamic mechanical testing with a dynamic mechanical analyzer (VA 4000, Metravib RDS, Limonest, France). The measurements were carried out in the bending mode, and the corresponding viscoelastic properties were determined as a function of temperature. The temperature used in this investigation was varied from 30 to 150°C with a heating rate of 10°C/min under nitrogen flow. The samples were scanned at a fixed frequency of 10 Hz with a static strain of 0.3% and a dynamic strain of 0.1%.

Rheological properties

Virgin PS and the nanocomposites were subjected to rheological measurements with a parallel-plate rheometer (RDA-3, Rheometrics, Nagoya, Japan). The measurements were conducted under a nitrogen atmosphere. The strain region in which the material could be regarded as linear viscoelastic was determined by amplitude experiments to the order of 10%. Isothermal frequency sweeps were carried out at different temperatures ranging from 140 to 220°C, and the master curves were generated with the Williams–Landel–Ferry equation.

Thermal properties

DSC. Samples of virgin PS and nanocomposites of 5 mg or less were scanned from 40 to 200°C under a nitrogen atmosphere for 5 min at a heating rate of 10°C/min with DSC (Diamond DSC, PerkinElmer, Waltham, MA). Subsequently, the samples were cooled to room temperature and reheated under similar conditions. The corresponding glass-transition temperature (T_g), based on the second scan, was recorded.

TGA. Virgin PS and the nanocomposites were subjected to TGA with a PerkinElmer Pyris-1 TGA apparatus. Samples of 5 mg or less were heated from 40 to 600°C at a heating rate of 10°C/min in a nitrogen atmosphere, and the corresponding weight loss was recorded.

RESULTS AND DISCUSSION

Morphology

XRD

Figure 1 displays the wide-angle XRD patterns of the nanoclays, Na-MMT, C20A, and OMMT. The d_{001}-spacing was calculated from the peak positions with Bragg's law, $2d \sin \theta = n\lambda$, where n is an integer determined by the order given, λ is the X-ray wavelength

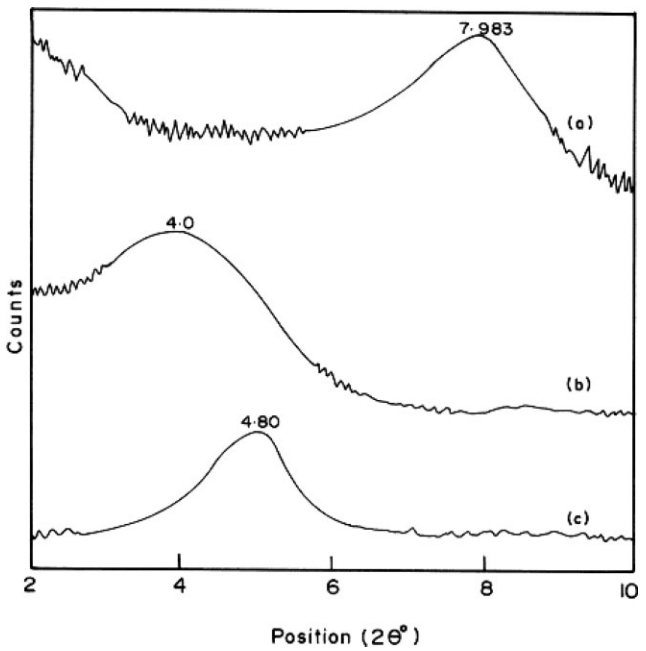

Figure 1 XRD patterns of (a) Na-MMT, (b) C20A, and (c) OMMT nanoclays.

(1.74 nm), *d* is the spacing between the planes in the atomic lattice, and θ is the angle between the incident ray and the scattering planes. Na-MMT [Fig. 1(a)] shows a diffraction peak at $2\theta = 7.98^\circ$ corresponding to a *d*-spacing of 1.28 nm. The XRD pattern of treated clay OMMT [Fig. 1(c)] reveals a reflection peak at $2\theta = 4.8^\circ$ with a *d*-spacing of 1.84 nm. This resultant increase in the basal spacing confirms intercalation in the Na-MMT clay on modification with STAC. Similarly, the XRD pattern of the commercial clay [C20A; Fig. 1(b)] reveals a spectrum at 4.0° with a *d*-spacing of 2.42 nm, thus indicating intercalation in the treated clay in the presence of di(hydrogenated tallow alkyl) dimethyl ammonium chloride as a surfactant. The resultant increase in the *d*-spacing in the case of C20A versus OMMT can be attributed to an increase in the alkyl chain length of the organic surfactant, which results in a random packing arrangement of the chains within the clay layers.[28–31]

In the case of Na-MMT/PS nanocomposites [Fig. 2(a)], the XRD pattern displays an increase in the intergallery spacing to about 3.47 nm with a peak at 2.95°. This increase in the intergallery spacing is probably due to intercalation of PS chains between the clay platelets. Conversely, the treated nanocomposites [Fig. 2(c)] prepared with the C20A nanoclay revealed an absence of any basal reflections in the XRD patterns. The nanocomposites may have formed as exfoliated nanocomposites in which the organoclay was delaminated and dispersed in the polymer matrix. The deletion of the peaks from the XRD patterns does not indicate complete exfoliation of the clay galleries.[25] The detailed morphology is further corroborated by the TEM analysis discussed in the next section.

However, a secondary peak at $2\theta = 8.040^\circ$ with a *d*-spacing of 1.2 nm was noticed in the case of OMMT/PS nanocomposites [Fig. 2(b)], indicating the presence of a small amount of the treated clay that remained unexfoliated in PS and existed in the form of an intercalated layered structure. Similar behavior was also reported by Wang et al.[26] for PS/MMT nanocomposites with a long-chain intercalating agent.

TEM

The nanometer-scale dispersion of the Na-MMT, OMMT, and C20A nanoclays within the PS matrix is further corroborated by TEM images depicted in Figure 3(a–c), respectively. The lighter portion represents PS, with the dark lines corresponding to silicate layers. In comparison with the pristine clay, the interlayer expansion clearly shows the intercalation of polymer chains in the interlayer region. However, the ordered lamellar structure of Na-MMT tactoids is still maintained as depicted in Figure 3(a). Furthermore, this also confirms that Na-MMT clay remains a microcomposite or conventional composite, and this can be explained by the fact that the polar nature of the clay hinders the wetting of the polymer over the clay surface. Conversely, in the case of the nanocomposites prepared with the organically modified clay (OMMT), exfoliated silicate layers [Fig. 3(b)] within the PS matrix as well as layers with an intercalated morphology were observed. This behavior further shows the

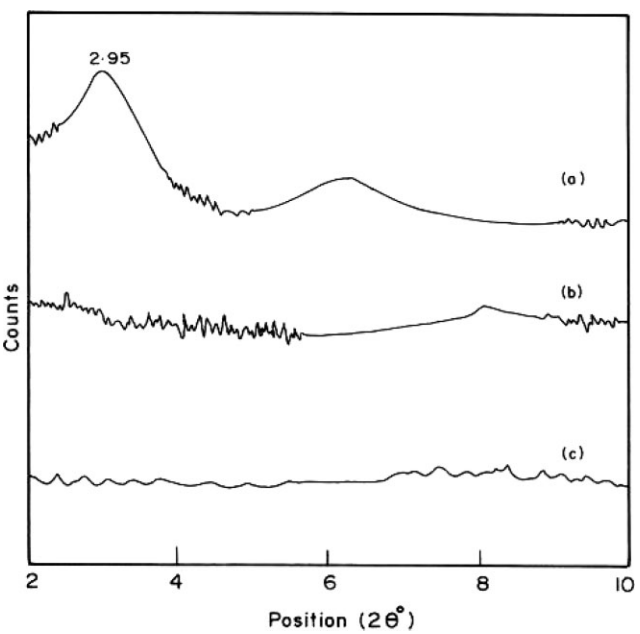

Figure 2 XRD patterns of (a) Na-MMT/PS, (b) OMMT/PS, and (c) C20A/PS nanocomposites at a 5% clay loading.

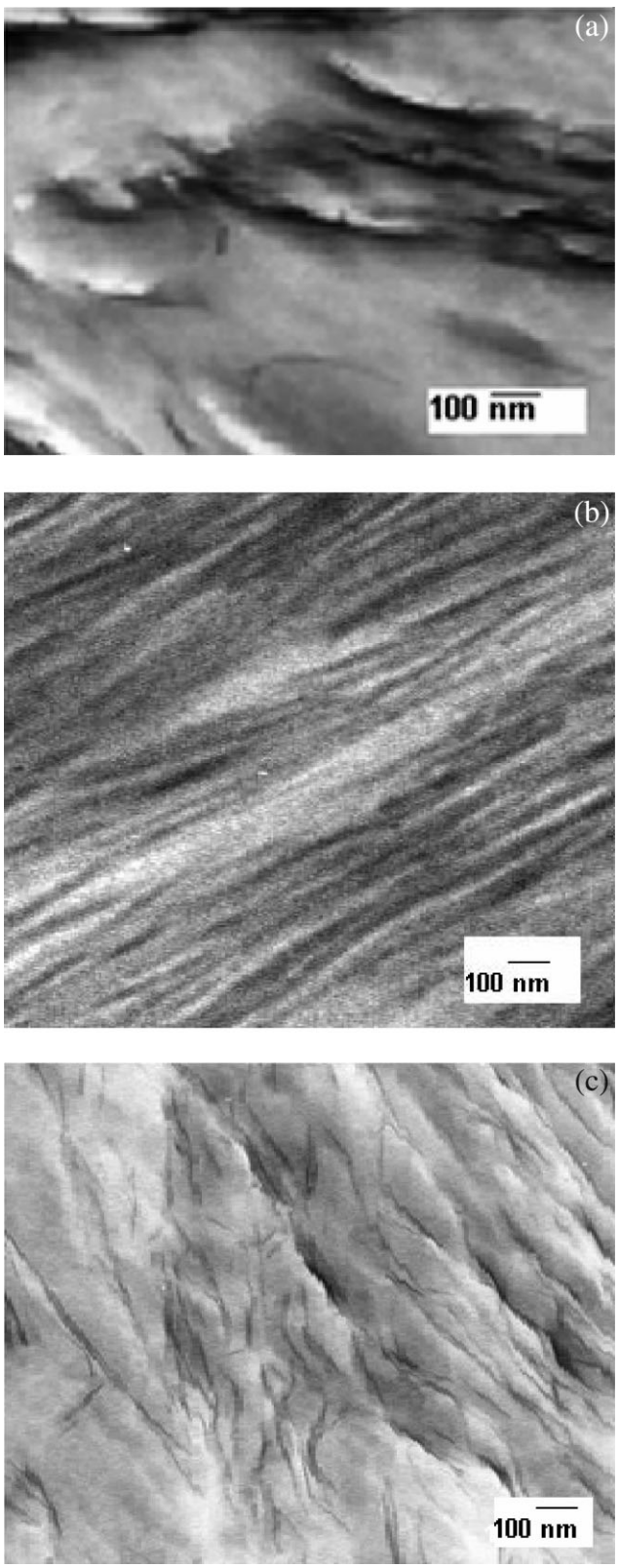

Figure 3 TEM micrographs of (a) Na-MMT/PS, (b) OMMT/PS, and (c) C20A/PS nanocomposites at a 5% clay loading.

presence of STAC as a surfactant, which considerably altered the surface chemistry of the polar Na-MMT clay. Similarly, C20A/PS nanocomposites, as enumerated in Figure 3(c), also exhibited a combination of intercalated and exfoliated structures of the clay layers. The absence of a diffraction peak in XRD implies delamination of the clay tactoids. Individual clay platelets were distributed uniformly in the PS matrix. However, in comparison with OMMT nanocomposites, the extent of the exfoliation was greater in the case of the C20A/PS system, and this further confirms that the modification of the clay with di(hydrogenated tallow alkyl) dimethyl ammonium chloride lowered electrostatic interactions between the clay layers and enlarged their intragallery spacing, thus facilitating exfoliation and efficient dispersion of the clay.[20]

Mechanical properties

Tensile properties

The tensile properties of virgin PS and the nanocomposites as a function of the clay loading are presented in Table I. With an increase in the clay loading from 1 to 5%, there was a progressive increase in the tensile strength and modulus of the nanocomposites. The nanocomposites prepared with organically modified clays C20A and OMMT showed higher tensile strength and modulus than the Na-MMT/PS nanocomposites. Increases of 62.18 and 83.3% in the tensile strength and 25.9 and 27.5% in the modulus of PS were obtained with the incorporation of 5 wt % concentrations of OMMT and C20A nanoclays, respectively. The primary cause for such improvement is probably the presence of immobilized or partially mobilized polymer phases as a result of the interaction of polymer chains with the organic modification of the clays and the large number of interacting molecules due to the dispersed phase volume ratio characteristic of largely exfoliated nanocomposites. It is also likely that the silicate layer orientation and molecular orientation along the flow (tensile) direction significantly contributed to the observed reinforcement effects.[17] C20A/PS nanocomposites at a 5% clay loading exhibited optimum performance. However, the enhancement of modulus was reasonably ascribed to the high resistance exerted by the clay platelets against the plastic deformation and stretching resistance of the oriented polymer backbones in the galleries. Similar observations were also reported by Uthirakumar et al.[32] for a PS/clay nanocomposite prepared by an *in situ* polymerization technique. The improvement in the tensile properties of the matrix polymer with the incorporation of Na-MMT and organically modified OMMT and C20A clays is also graphically represented in Figure 4(a,b), respectively.

TABLE I
Effect of the Clay Loading on the Tensile Properties

Sample type	Clay content (%)	Tensile strength (MPa)	SD	Tensile modulus (MPa)	SD	Elongation (%)	SD
PS	0	24.12	0.97	845	0.74	1.60	1.09
Na-MMT/PS	1	27.36	1.02	959	1.13	0.97	1.10
	3	31.27±1.02[a]	0.86	1001±1.44	1.01	0.82±1.17	0.97
	5	32.70	0.85	1023	1.08	1.07	1.13
	7	29.65	0.99	998	1.10	1.00	0.99
C20A/PS	1	37.95±1.02	0.81	980	0.78	0.85±1.11	1.02
	3	43.39	0.88	1065	0.96	0.72	0.98
	5	44.23	0.79	1078±1.21	1.05	0.99	0.89
	7	40.90	0.67	1056	1.00	1.76	0.78
OMMT/PS	1	34.21	0.86	968	1.02	1.11±1.03	1.21
	3	37.83	1.02	1042±1.02	1.11	0.99	1.08
	5	39.12±1.08	1.05	1064	0.98	0.80	1.02
	7	34.54	1.01	1024	0.87	0.99	0.98

Measurement uncertainty values are reported according to American Association for Laboratory Accreditation guidelines.[37] SD = standard deviation.

As evident in other reinforced plastics, the elongation at break showed a sequential decrease with the addition of the clay.

Nevertheless, with a further increase in the nanoclay loading from 5 to 7%, a marginal decrease in the tensile strength and modulus of the nanocomposites was observed. This behavior can probably be attributed to the filler–filler interaction, which results in agglomerates and induces local stress concentration in the nanocomposites, which leads to a reduction in the clay aspect ratio, thereby reducing the contact surface between the organoclay and the polymer matrix.[33] Thus, the nanocomposites at a higher clay loading (i.e., 7 wt %) exhibited lower tensile strength and modulus when subjected to tensile mode deformation.

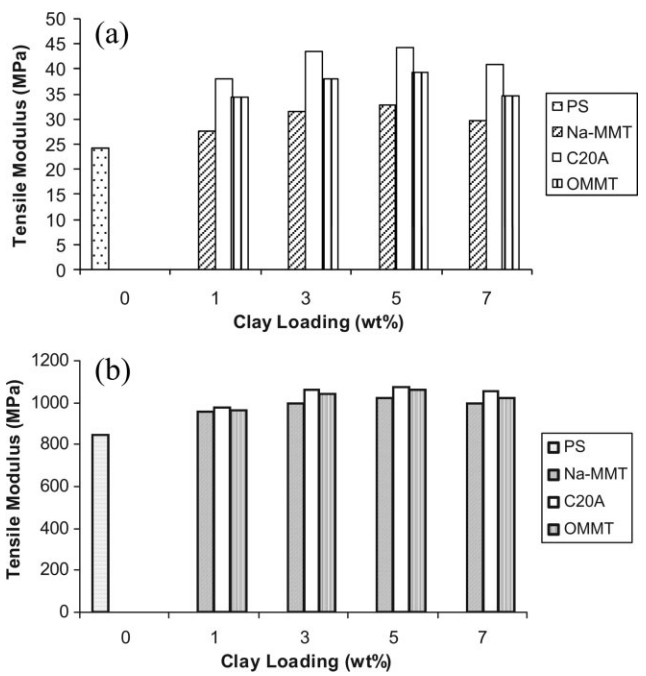

Figure 4 Effect of the clay loading on (a) the tensile strength and (b) the tensile modulus of the nanocomposites.

Flexural properties

The variation of the flexural strength and modulus with the clay loading is summarized in Table II. It was observed that the addition of the Na-MMT nanoclay led to a phenomenon similar to that observed for tensile properties. This was probably due to the incompatibility of the dispersed polar clay within the nonpolar matrix polymer. However, organic modification of Na-MMT resulted in improved performance of the nanocomposite. C20A/PS and OMMT/PS nanocomposites showed improved flexural properties at all compositions in comparison with virgin PS and Na-MMT/PS nanocomposites.

TABLE II
Effect of the Clay Loading on the Flexural Properties

Sample type	Clay content (%)	Flexural strength (MPa)	SD	Flexural modulus (MPa)	SD
PS	0	29.03	0.63	2719	0.62
Na-MMT/PS	1	31.56	0.78	2796±1.35	1.12
	3	32.37	0.81	2801	1.03
	5	36.15±1.2	0.93	2845	0.78
	7	25.43	0.88	2645	0.79
C20A/PS	1	40.97	1.08	2843	0.48
	3	42.83	0.89	2877	0.96
	5	44.96±1.01	1.03	3030±1.21	1.01
	7	38.97	1.09	2788	0.99
OMMT/PS	1	34.82	0.99	2832±1.01	1.13
	3	39.89±1.22	1.01	2943	1.02
	5	41.43	1.02	2985	0.97
	7	38.67	1.01	2899	0.99

SD = standard deviation.

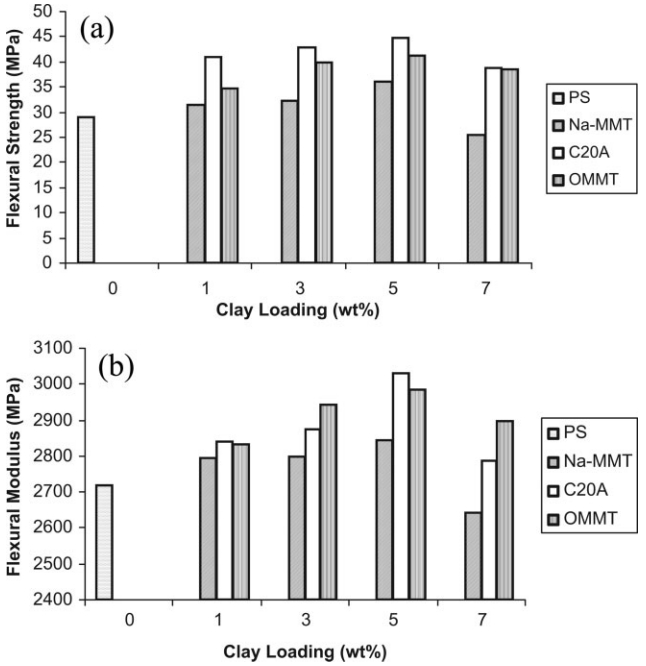

Figure 5 Effect of the clay loading on (a) the flexural strength and (b) the flexural modulus of the nanocomposites.

The flexural strength and modulus increased by 54.87% and 11.4%, respectively, in the case of C20A/PS nanocomposites at a 5% clay loading in comparison with virgin PS. This increase in the flexural strength and modulus was probably due to exfoliation of the clay resulting in a larger polymer/clay interfacial area and thereby retarding plastic deformation. The increase in the flexural strength and modulus of the PS matrix in the nanocomposites is graphically illustrated in Figure 5(a,b).

TABLE III
Effect of the Clay Loading on the Impact Strength

Sample type	Clay content (%)	Impact strength (J/m)	SD
PS	0	22.46	0.59
Na-MMT/PS	1	23.48	0.71
	3	30.84	1.13
	5	32.78±1.02	1.01
	7	29.78	0.89
C20A/PS	1	25.72±1.47	1.24
	3	37.43	0.96
	5	39.05	1.12
	7	35.67	1.09
OMMT/PS	1	24.03±1.20	1.13
	3	31.76	1.12
	5	38.24	1.02
	7	30.78	1.09

SD = standard deviation.

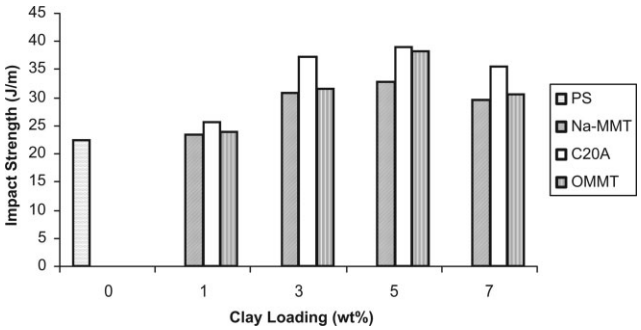

Figure 6 Effect of the clay loading on the impact strength of the nanocomposites.

Impact strength

The impact strength of virgin PS and the nanocomposites is depicted in Table III and Figure 6. It is evident that the impact strength of the PS matrix increased progressively with the incorporation of the nanoclays. This was due to the reinforcing effect of the nanoscale filler within the matrix network because of the intercalation of polymer chains through galleries of the nanoclays.[34] Furthermore, OMMT and C20A/PS nanocomposites exhibited improved impact strength in comparison with both the virgin matrix and Na-MMT/PS nanocomposites. C20A/PS nanocomposite prepared at a 5% clay loading showed optimum strength. An approximately 73.86% increase in the impact strength in comparison with the virgin matrix was noticed. This phenomenon further confirmed the efficient dispersion of treated clays in the presence of di(hydrogenated tallow alkyl) dimethyl ammonium chloride as a surfactant, which resulted in improved interfacial adhesion between the dispersed clay and the matrix polymer.

Because the composites prepared with a 5% clay loading showed optimum mechanical performance, these nanocomposites along with the virgin matrix were taken for further characterization studies.

DMA

Storage modulus (E')

The elastic component (E') is a measure of the load-bearing capacity of a material and is analogous to the flexural modulus, being determined in accordance with ASTM D 790. The variation of E' of virgin PS and the nanocomposites as a function of temperature is presented in Figure 7. The addition of organically modified nanoclays (C20A and OMMT) substantially increased the modulus of the virgin matrix in both glassy and rubbery regions. This indicated the reinforcing effect imparted by nanoclays along with the high aspect ratio of the clay platelets, which allowed a greater degree of stress transfer at the interface.[35]

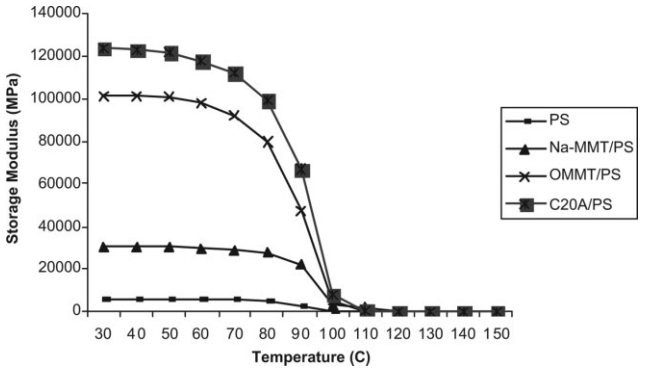

Figure 7 E' of (a) PS, (b) Na-MMT/PS, (c) OMMT/PS, and (d) C20A/PS nanocomposites at a 5% clay loading. [Color figure can be viewed in the online issue, which is available at www.interscience.wiley.com.]

Furthermore, restricted segmental motion at the organic–inorganic interface due to confinement of the polymeric chains inside the clay galleries at the nanoscale level may be the cause of the phenomenal increase in E'. Similar behavior was investigated by Uthirakumar et al.[32] for PS/MMT nanocomposites. An increase in E' of virgin PS by 1.2 times with the addition of 1% MMT was reported. However, the incorporation of Na-MMT could not substantially enhance the modulus of PS, and this could be primarily attributed to its polar nature, which resulted in incompatibility with the matrix polymer.

C20A/PS nanocomposites exhibited the optimum magnitude of E', thus revealing exfoliation of the clay galleries leading to efficient dispersion of the clay platelets in the matrix polymer.

Damping factor (tan δ)

The variation of tan δ as a function of temperature is enumerated in Figure 8. The tan δ curves represent the ratio of dissipated energy to the stored energy. T_g values of the virgin polymer and the nanocomposites were determined from the peak values of tan δ. It is evident from Figure 8 that the incorporation of the nanoclays shifted T_g of the PS matrix to higher temperature regions, and this is in agreement with the DSC results discussed in later sections. This behavior is probably attributable to segmental immobilization of matrix chains in the presence of nanoscale clay platelets.[34] In the case of organically modified clay nanocomposites (OMMT/PS and C20A/PS), marginally higher T_g values and broadening of the transition region were observed in comparison with the Na-MMT/PS clay nanocomposites, and this may be ascribed to its exfoliation morphology leading to a large surface area of the clay interacting with the polymer. T_g values corresponding to DMA measurements were 20° higher, as observed from DSC thermograms.

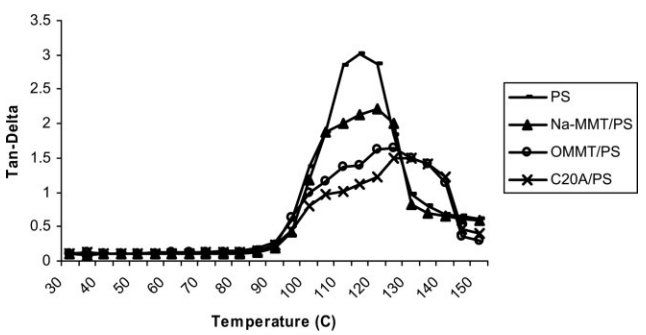

Figure 8 Tan δ of (a) PS, (b) Na-MMT/PS, (c) OMMT/PS, and (d) C20A/PS nanocomposites at a 5% clay loading.

Rheological properties

The variation of the storage modulus (G') as a function of the angular frequency (ω) is presented in Figure 9. The master curves of virgin PS and the nanocomposites were generated by the application of the time–temperature superposition principle. Both frequency (horizontal) and modulus (vertical) shift factors (a_T and b_T, respectively) were applied simultaneously to the data to create master curves. A reference temperature of 180°C was selected, and the frequency shift factors were fitted to the Williams–Landel–Ferry equation:

$$\text{Log } a_T = -c_1(T - T_0)/c_2 + (T - T_0) \qquad (1)$$

where c_1 (5.3 K) and c_2 (122 K) are constants, T is the temperature, and T_0 is the reference temperature.

As evident from Figure 9, G' increased with the increase in frequency in all the samples. In the case of the nanocomposites, the master curves exhibited three distinct regions from a high frequency to a low

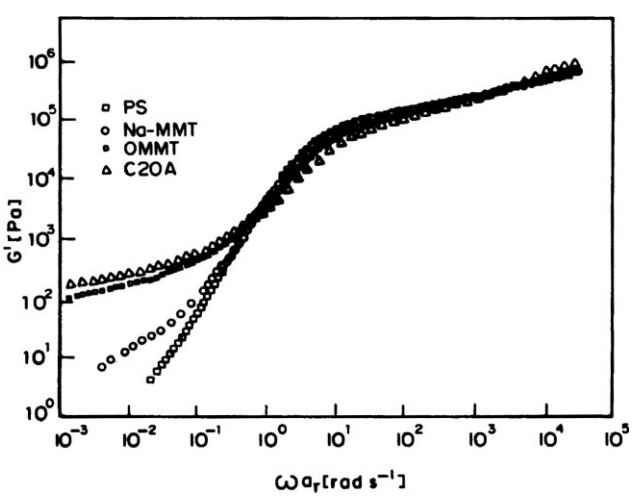

Figure 9 Variation of G' as a function of ω for (a) PS, (b) Na-MMT/PS, (c) OMMT/PS, and (d) C20A/PS nanocomposites at a 5% clay loading.

frequency: glassy, plateau, and terminal. At low-frequency terminal regions ($10^{-3} < \omega a_T < 10^{\circ}$), the formation of a shoulder in G' was observed in the treated nanocomposites (OMMT and C20A). This indicated the formation of a network-like superstructure in these nanocomposites. However, in the case of the nanocomposites prepared with Na-MMT, the existence of a network structure was less in comparison with the treated nanocomposites, and this was probably due to the weak interaction between the silicate layers in the polar clay.

The plateau region showed a thinning effect in the organically modified nanocomposites. This behavior was probably due to a more exfoliated structure of the layered silicate in the C20A/PS nanocomposites, which is clearly evident from TEM and XRD measurements. It is also likely that the nanocomposite consisted of individual hairy platelets, with the surfactant molecule ionically bonded to the surface of the platelets. The fine dispersion of these hairy platelets was expected to cause a thinning effect due to the interaction of the hairs with the matrix polymer. Similar behavior was also expected in OMMT/PS nanocomposites, in which the thinning effect was marginally less in comparison with the C20A/PS system. However, a thinning effect was absent in Na-MMT nanocomposites, in which stacks of clay layers dispersed in the PS matrix were observed from morphological investigations.[36]

At high-frequency transition regions, G' of the C20A nanocomposites increased, thus revealing an improved exfoliated structure of the hairy platelets within the PS matrix. A similar increase in G' of the PS matrix in the OMMT nanocomposites was also observed, indicating the presence of stearyl trimethyl ammonium chloride as a surfactant.

However, the magnitude of the increase in G' was higher in the C20A nanocomposites in both the low-frequency, glassy region and the high-frequency, terminal flow region, confirming the effectiveness of di(hydrogenated tallow alkyl) dimethyl ammonium chloride as a surfactant, which resulted in improved interfacial adhesion between the dispersed clay and the matrix polymer.

Thermal properties

DSC

The DSC thermograms of virgin PS and the nanocomposites are presented in Figure 10. It is evident that the virgin polymer [Fig. 10(a)] exhibited an endothermic peak at about 96°C, which probably corresponded to T_g of the matrix. However, with the incorporation of nanoclays [Na-MMT, OMMT, and C20A; Fig. 10(b–d)], there was a shift in the T_g of the PS matrix to about 102, 105, and 107°C, respectively. This increase

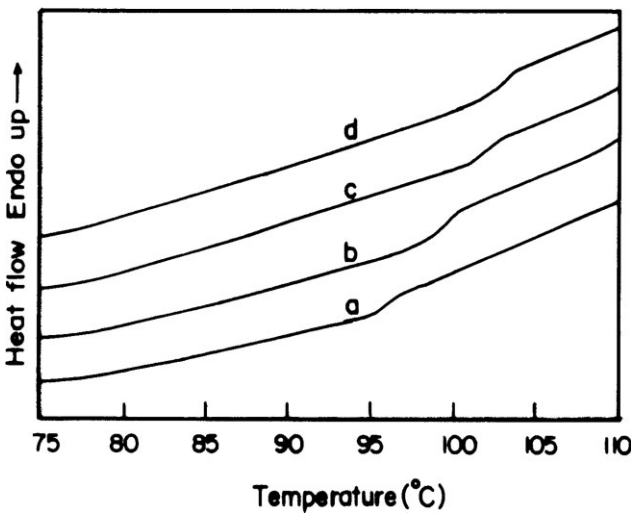

Figure 10 DSC thermograms of (a) PS, (b) Na-MMT/PS, (c) OMMT/PS, and (d) C20A/PS nanocomposites at a 5% clay loading.

in T_g was probably due to a retarding effect of clay platelets on the segmental motions of the polymer chains at the organic–inorganic interface. Furthermore, the confinement of PS chains between the silicate layers as well as silicate surface–polymer interactions in the nanostructured hybrids resulted in an enhancement of T_g of the virgin matrix. Similar observations were reported by Kim et al.[30] for PS/clay nanocomposites prepared with the solvent-casting method. PS/MMT nanocomposites containing 30 wt % MMT and prepared by emulsion polymerization also exhibited an improvement in the T_g of the PS matrix to ~ 5°C.[26] The majority of other well-dispersed polymer/clay nanocomposites also exhibited higher T_g values than their corresponding pristine polymers.[31]

TGA

The thermal degradation behavior of virgin PS and the nanocomposites is presented in Figure 11. It is evident that the degradation temperature of the virgin matrix increased with the incorporation of the nanoclays. The improvement in the degradation temperature was probably due to the homogeneous dispersion of the silicate nanoplatelets in the PS matrix. The degradation temperature of the virgin matrix [Fig. 11(a)] was observed around 425°C, and it showed a marginal increase with the addition of 5 wt % Na-MMT nanoclay [Fig. 11(b)]. However, there was a substantial increase in the thermal stability of the C20A/PS nanocomposites [Fig. 11(d)]. The organically modified nanocomposites exhibited higher degradation temperatures [Fig. 11(d,e)] than the virgin PS and Na-MMT/PS. This noticeable increase in the degradation temperature mainly resulted from the dispersed nanoscale silicate layers, which

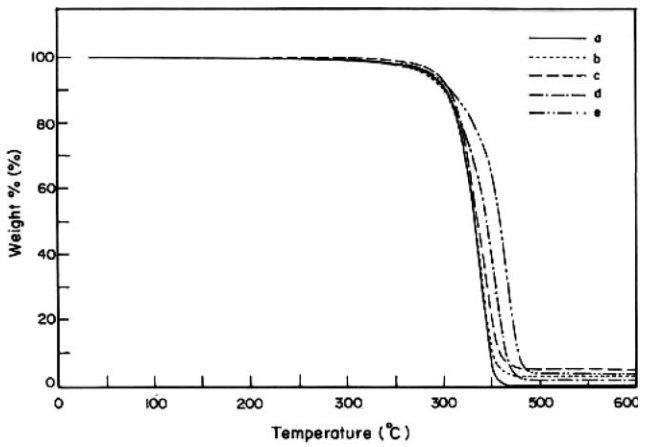

Figure 11 TGA of (a) PS, (b) Na-MMT/PS, (c) OMMT/PS, and (d) C20A/PS nanocomposites at a 3 wt% clay loading, and (e) C20A/PS nanocomposited at 3 wt% clay loading.

hindered the permeability of volatile decomposition products out of the material.[26]

CONCLUSIONS

The experimental findings revealed a consistent improvement in the mechanical properties of PS/layered silicate nanocomposites with a lower clay loading (5%) due to the reinforcing and toughening effect of nanoparticles. Morphological observations confirmed the efficient dispersion of the nanoclays and intercalation of the polymer segments in the gallery space in the case of organically modified nanocomposites. DMA showed an increase in the storage modulus and loss modulus with the addition of C20A and OMMT nanoclays into the PS matrix. Tan δ curves also showed marginal increases in T_g in the case of the nanocomposites. The melt rheology of the nanocomposites prepared with organically modified clays displayed three distinct regions—glassy, plateau, and terminal—from a high-frequency region to a low-frequency region, with increased G' in the glassy and terminal regions. A DSC thermogram showed a marginal increase in T_g of the PS matrix in the nanocomposites. The thermal stability of the matrix polymer also increased with the incorporation of the nanoclays. Thus, PS/layered silicate nanocomposites can be commercially exploited with an optimal nanoclay loading. Future research will be primarily concentrated on altering the surface chemistry of natural MMT to attain improved properties.

References

1. Kim, T. H.; Jang, L. W.; Lee, C. D.; Choi, H. J.; Jhon, M. S. Macromol Rapid Commun 2002, 23, 191.
2. Yeh, J. M.; Liou, S. J.; Lai, C. Y.; Wu, P. C. Chem Mater 2001, 13, 1131.
3. Yeh, J. M.; Liou, S. J.; Lai, C. Y.; Wu, P. C. Chem Mater 2002, 14, 154.
4. Strawhecker, K. E.; Manias, E. Chem Mater 2000, 12, 2943.
5. Wang, D.; Zhu, J.; Yao, Q.; Wilkie, C. A. Chem Mater 2002, 14, 3837.
6. Kim, Y. K.; Choi, Y. S.; Wang, K. H.; Chung, I. J. Chem Mater 2002, 14, 4990.
7. Cho, J. W.; Paul, D. R. Polymer 2001, 42, 1083.
8. Yano, K.; Usuki, A.; Karauchi, T.; Kamigaito, O. J Polym Sci Part A: Polym Chem 1993, 31, 2493.
9. Kim, G. M.; Lee, D. H.; Hoffmann, B.; Kressler, J.; Stoppelmann, G. Polymer 2001, 42, 1095.
10. Wang, Y.; Suna, A.; Mahler, W.; Kawoski, R. J Chem Phys 1997, 87, 7315.
11. Xu, X.; Qutubuddin, S. Polymer 2001, 42, 807.
12. Wanjale, S. D.; Jog, J. P. J Appl Polym Sci 2003, 90, 3233.
13. Wan, C.; Qiao, X.; Zhang, Y. J Appl Polym Sci 2003, 89, 2184.
14. Reichert, P.; Nitz, H.; Klinke, S.; Brandsch, R.; Thomann, T.; Mulhaupt, R. Macromol Mater Eng 2000, 8, 275.
15. Tjong, S. C.; Bao, S. P. J Polym Sci Part B: Polym Phys 2004, 42, 2878.
16. Devaux, E.; Bourbigot, S.; Achari, A. E. J Appl Polym Sci 2002, 86, 2416.
17. Zhang, Q. X.; Yu, Z. Z.; Yang, M.; Ma, J.; Mai, Y. W. J Polym Sci Part B: Polym Phys 2003, 41, 2861.
18. Vaia, R. A.; Ighi, H.; Giannelis, E. P. Chem Mater 1993, 5, 1694.
19. Lim, Y. T.; Park, O. O. Rheo Acta 2001, 40, 220.
20. Parija, S.; Nayak, S. K.; Verma, S. K.; Tripathy, S. S. Polym Compos 2004, 25, 646.
21. Salahuddin, N.; Shehata, M. Polymer 2001, 42, 8379.
22. Bandyopadhyay, S.; Giannelis, E. P.; Hsieh, A. Polym 2000, 82, 208.
23. Kato, C.; Kuroda, K.; Takahara, H. Clay Clay Miner 1981, 29, 294.
24. Akelah, A.; Moet, A. J Mater Sci 1996, 31, 3189.
25. Xaoan, F.; Syed Q. Mater Lett 2000, 42, 12.
26. Wang, D.; Zhu, J.; Yao, Q.; Wilkie, A. A. Chem Mater 2002, 14, 3837.
27. Tanque, S.; Utracki, L. A.; Garcia-Rejon, A.; Sammut, P.; Ton-That, M. T.; Pesneau, I.; Kamal, M. R.; Lyngaae-Jorgensen, J. Polym Eng Sci 2004, 44, 1061.
28. Hwu, J. M.; Ko, T. H.; Yang, W. T.; Lin, J. C.; Jiang, G. J.; Xie, W.; Pan, W. P. J Appl Polym Sci 2004, 91, 101.
29. Wang, H. W.; Chang, K. C.; Chu, H. C.; Liou, S. J.; Yeh, J. M. J Appl Polym Sci 2004, 92, 2402.
30. Kim, T. H.; Lim, S. T.; Lee, C. H.; Choi, H. J.; Jhon, M. S. J Appl Polym Sci 2003, 87, 2106.
31. Fu, X.; Qutubuddin, S. Mater Lett 2000, 42, 12.
32. Uthirakumar, P.; Song, M. K.; Nah, C.; Lee, Y. S. Eur Polym J 2005, 41, 211.
33. Rong, M. Z.; Zhang, M. Q.; Zhang, Y. X.; Zeng, H. M.; Walter, R.; Friedrich, K. Polymer 2001, 42, 167.
34. Kurokawa, Y.; Yusuda, H.; Oia, A. J Mater Sci Lett 1996, 15, 1481.
35. Hasegawa, O. H.; Kawasumi, M.; Usuki, A. J Appl Polym Sci 1999, 74, 3359.
36. Meincke, O.; Hoffmann, B.; Dietrich, C.; Friedrich, C. Macromol Chem Phys 2003, 204, 823.
37. Thomas, M. A. A2LA Guidelines for Estimation of Measurement Uncertainty in Testing; American Association for Laboratory Accreditation: Frederick, MD, 2002; p 1.